Acta Biomaterialia xxx (xxxx) xxx

Contents lists available at ScienceDirect

Acta Biomaterialia

journal homepage: www.elsevier.com/locate/actbio

Short communication

Tissue-adhesive hydrogel for multimodal drug release to immune cells in skin

Nicole B. Day[a], Rianne Dalhuisen[a,b], Nichole E. Loomis[a], Sarah G. Adzema[a], Jai Prakash[b], C. Wyatt Shields IV[a,c,*]

[a] Department of Chemical and Biological Engineering, University of Colorado Boulder, Boulder CO 80303, United States
[b] Department of Advanced Organ Bioengineering and Therapeutics, Section: Engineered Therapeutics, University of Twente, Enschede, the Netherlands
[c] Biomedical Engineering Program, University of Colorado Boulder, Boulder CO 80303, United States

ARTICLE INFO

Article history:
Received 12 April 2022
Revised 21 July 2022
Accepted 27 July 2022
Available online xxx

Keywords:
Hydrogel
Drug delivery
Immunotherapy
Microparticles
Macrophage polarization

ABSTRACT

Both innate and adaptive immune systems play a crucial role in the pathology of skin diseases. To control these cells, there is a need for transdermal drug delivery systems that can target multiple cell populations at independently tunable rates. Herein, we describe a tissue-adhesive hydrogel system that contains particles capable of regulating the release of small molecule drugs at defined rates. Resiquimod (a macrophage-targeting drug) and palbociclib (a T cell-targeting drug) are encapsulated within two types of silicone particles embedded within the hydrogel. We demonstrate that drug release is mediated by the crosslink density of the particles, which is decoupled from the bulk properties of the hydrogel. We show that this system can be used to sustainably polarize macrophages toward an anti-tumor phenotype *in vitro* and *ex vivo*, and that the hydrogels can remain attached to skin explants for several days without generating toxicity. The hydrogel system is compatible with standard dermatological procedures and allows transdermal passage of drugs. The multimodal, tunable nature of this system has implications in treating a variety of skin disorders, managing infections, and delivering vaccines.

Statement of significance

We describe a tissue-adhesive hydrogel that can regulate the release of drugs in a manner that is decoupled from its bulk properties. The mechanism of drug release is mediated by embedded microparticles with well-defined crosslink densities. The significance of this system is that, by encapsulating different drugs into the particles, it is possible to achieve multimodal drug release. We demonstrate this capability by releasing two immunomodulatory drugs at disparate rates. A drug that targets innate immune cells is released quickly, and a drug that targets adaptive immune cells is released slowly. This programmable system offers a direct means by which cellular responses can be enhanced through independent targeting for a variety of transdermal applications, including cancer treatment and vaccine delivery.

1. Introduction

Advances in materials engineering have improved the performance of immunotherapies by prompting more potent and durable immune responses [1]. However, the controlled release of drugs to the skin at independently tunable rates remains a challenge. This is especially important for activating different populations of immune cells. Contributing factors include poor penetration of drugs through the stratum corneum, limited control over their release from standard ointments and creams, and poor patient compliance in response to adverse effects. Hydrogels are gaining popularity as a platform for addressing these factors due to their biocompatibility, flexible chemistry, and mechanical similarity to living tissues

Abbreviations: R848, Resiquimod; Plb, Palbociclib; DMSO, Dimethyl sulfoxide; TLR, Toll-like receptor; CDK, Cyclin-dependent kinase; DMEM, Dulbecco's modified Eagle's medium; DPBS, Dulbecco's phosphate buffered saline; TEMED, Tetramethylethylenediamine; TEA, Triethylamine; TMOS, Tetramethyl orthosilicate; DMODMS, Dimethoxydimethylsilane; PVA, Poly(vinyl alchohol); OCT, Optimal cutting temperature; FBS, Fetal bovine serum; LCDS, Low crosslink density silicone; PDMS, Polydimethylsiloxane; HCDS, High crosslink density silicone; TCM, Tumor-conditioned media; UV-UPLC, Ultraviolet ultra-performance liquid chromatography; SEM, Scanning electron microscopy; PAM, Polyacrylamide; iNOS, Inducible nitric oxide synthase; Arg-1, Arginase-1; CD, Cluster of differentiation; MHCII, Major histocompatibility complex class II.

* Corresponding author.
E-mail address: Charles.Shields@colorado.edu (C.W. Shields IV).

https://doi.org/10.1016/j.actbio.2022.07.053
1742-7061/

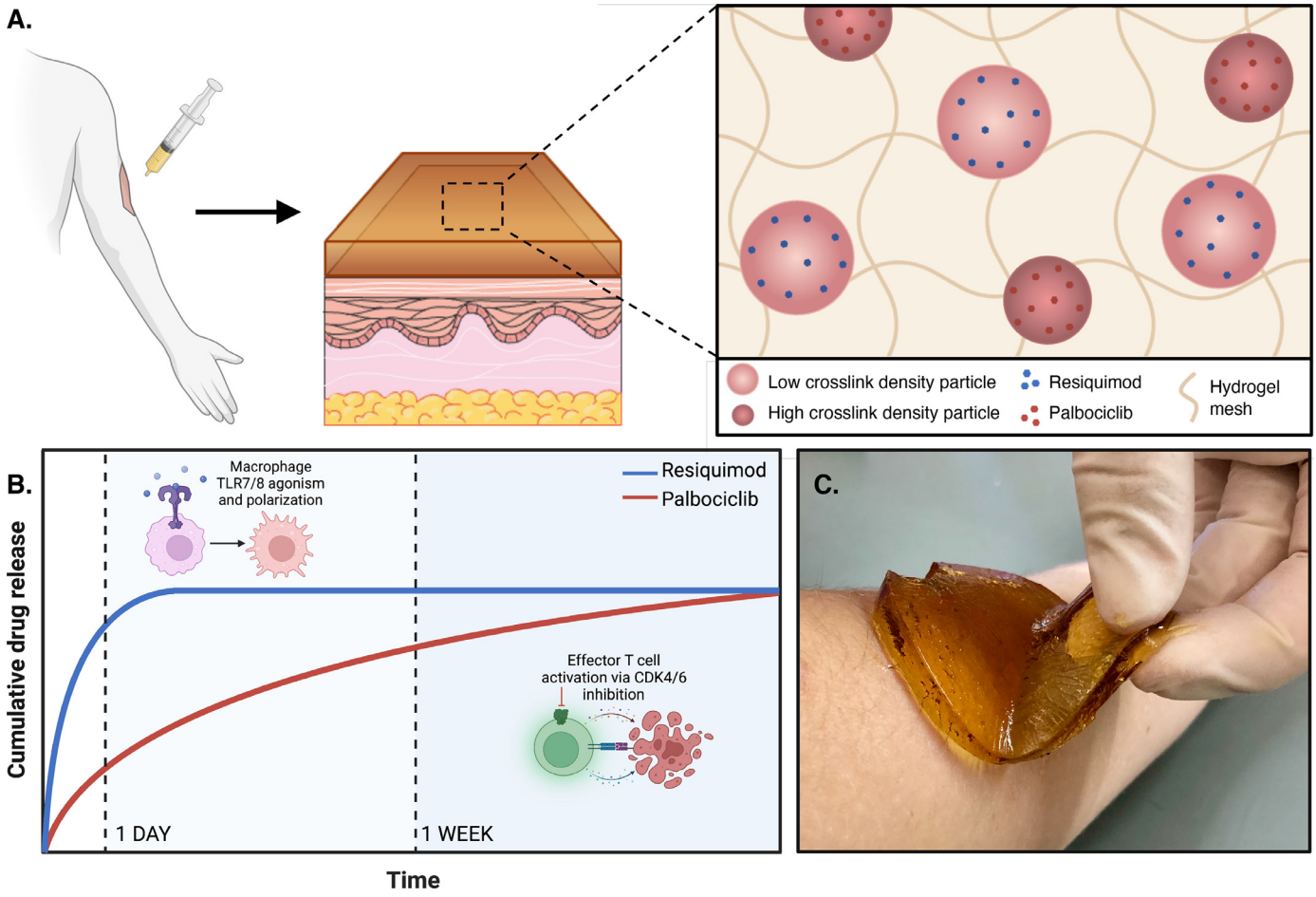

Fig. 1. Overview of the tissue-adhesive hydrogel system for multimodal drug release. A) A hydrogel embedded with drug-containing microparticles (i.e., with low or high crosslink densities) adheres to skin. Two immunomodulatory drugs, resiquimod and palbociclib, are released from the microparticles at rates commensurate with their respective immune cell activation timelines. B) Resiquimod is released quickly due to low particle crosslink densities; palbociclib is released slowly due to high particle crosslink densities. Illustrations show resiquimod inducing M1 macrophage polarizations by TLR7/8 agonism and palbociclib promoting cytotoxic T cell activation by CDK4/6 inhibition. C) Photograph of the adhesive hydrogel vehicle attached to skin.

[2,3]. However, the mechanisms governing drug release from hydrogels are often inextricably linked to the bulk properties of the hydrogel, making it difficult to tune network properties without affecting drug release kinetics [4]. Other hydrogel systems have been developed to release drugs at tunable rates; however, these systems either depended on stimuli-responsiveness to regulate drug release [5,6], which is not conducive for multimodal drug release, or lacked a simple means of synthesis for translational readiness [7–9]. There remains a need for a simple and versatile transdermal delivery system that enables multimodal drug release.

Herein, we describe a tissue-adhesive hydrogel embedded with microparticles that enable tunable release of encapsulated drugs in a manner that is decoupled from the bulk properties of the hydrogel (Fig. 1). While many implanted drug reservoirs aim to degrade over time, this hydrogel is designed as a flexible, biostable, and fully removable unit to sustainably deliver localized treatments while adherent, after which it can be painlessly peeled off, avoiding potentially adverse effects associated with materials degradation such as pH changes to the skin, bioresorption, and the formation of foreign body granulomas [10,11]. Hydration of the hydrogel can be maintained while adhered to skin through simple methods such as periodically depositing water on top to prevent drying out. Use of a detachable hydrogel also enables the incorporation of a range of engineered particle types to guide drug release without dependence on particle degradability, long-term biocompatibility, and repeated injections. Anchoring of such particles to the hydrogel network prevents their accumulation in tissues, a common fate of injected drug carriers [12,13]. Drug permeability through the skin can be enabled through standard dermatological procedures, such as by affixing the hydrogel within a surgical bed or a microneedle-treated site. These methods can enable lower doses of drugs to be dispensed over longer durations, improving therapeutic efficacies and reducing toxicities [14,15].

To demonstrate utility of this programmable hydrogel system—which we define as the hydrogel vehicle and embedded microparticles—we encapsulate and release two drugs used for melanoma immunotherapy at independently tuned rates. Specifically, we release resiquimod and palbociclib at different rates by adjusting the crosslink density of the particles encapsulating them. Resiquimod (R848) and palbociclib (Plb) are hydrophobic drugs with molecular weights of 314 and 448 Da, respectively, and solubilities of 31.4 and 13.0 mg/mL in dimethyl sulfoxide (DMSO). Resiquimod is a toll-like receptor (TLR)7/8-agonist that polarizes macrophages toward a proinflammatory (M1-like, herein referred to as “M1” for convenience) phenotype [16,17]. Palbociclib is a cyclin-dependent kinase (CDK)4/6-inhibitor that activates effector T cells and promotes their infiltration into solid tumors [18,19]. The combination of these drugs has the potential to elicit a potent immune response against residual and metastasizing tumor cells and prevent recurrence of molecularly similar tumors [16]. We therefore designed our hydrogel system to release resiquimod quickly (over several days) and palbociclib slowly (over several weeks) to

match the associated cell activation timescales (i.e., macrophages and T cells are members of the innate and adaptive immune systems, respectively). This proof-of-concept application highlights the independently tunable features of this hydrogel system for a range of uses such as treating actinic keratosis, dermatitis, and carcinoma as well as delivering analgesics, antibiotics, and vaccine components to the skin [20].

2. Materials and methods

2.1. Materials

RAW 264.7 murine macrophages and B16-F10 murine melanoma cells were sourced from the American Type Culture Collection (ATCC). BD Cytofix/Cytoperm fixation/permeabilization kit was obtained from BD Biosciences. Zombie Green Viability Kit was obtained from Biolegend. Dulbecco's modified Eagle's medium (DMEM) high glucose media, DMEM low glucose media, trypsin, and Dulbecco's phosphate buffered saline (DPBS) were obtained from Cytiva. Sylgard 184 Elastomer Curing Agent and Silicone Elastomer Base were obtained from Dow Chemical. Citramount medium was obtained from Electron Microscopy Sciences. Palbociclib was obtained from MedChemExpress. Hair depilating cream was obtained from Nair (Church & Dwight). Tetramethylethylenediamine (TEMED) and acetone were obtained from Millipore Sigma. Recombinant murine epidermal growth factor was obtained from Peprotech. Acrylamide, tannic acid, ammonium persulfate, *N,N'*-methylenebis(acrylamide), poly(ethylene glycol)-block-poly(propylene glycol)-block-poly(ethylene glycol) (Pluronic F108), Accumax, insulin, transferrin, 3,3–5′ triiodo-L-thyroxine, hydrocortisone, hydrochloric acid (HCl, 37%), triethylamine (TEA), tetramethyl orthosilicate (TMOS), dimethoxydimethylsilane (DMODMS), hexane, ethyl acetate, methanol, mineral oil, and poly(vinyl alcohol) (PVA) were obtained from Sigma-Aldrich. EasySep Mouse CD45 Positive Selection Kits were obtained from StemCell Technologies. Penicillin and streptomycin, mineral oil, DMSO, trifluoroacetic acid (TFA), acetonitrile (ACN), Dr. Maisch Reprosil-Pur 1.9 µm 120A C18-AQ media, optimal cutting temperature (OCT) embedding medium, BODIPY FL C_5 (4,4-Difluoro-5,7-Dimethyl-4-Bora-3a,4a-Diaza-*s*-Indacene-3-Pentanoic Acid), fetal bovine serum (FBS), UltraComp eBeads compensation beads, and anti-mouse CD16/CD32 Fc block were obtained from Thermo Fisher Scientific. See Supplemental Materials for details regarding fluorescent antibodies. Resiquimod was obtained from Tokyo Chemical Industry. Hematoxylin stain was obtained from Vector Laboratories. Glucose, PBS, Ham's F12 medium, penicillin-streptomycin, gentamicin sulfate salt, and Bambanker cell freezing media was obtained from VWR.

2.2. Particle synthesis and characterization

Low crosslink density silicone (LCDS) particles for encapsulating resiquimod were synthesized via homogenization of polydimethylsiloxane (PDMS) precursor and heat curing [21]. The precursor was prepared by mixing a total of 1 g of Sylgard 184 base and curing agent (crosslinker) in different mass ratios, followed by the addition of 250 µL 10 mg resiquimod / mL DMSO. Next, the PDMS mixture was added to 9 mL aqueous phase (15 wt.% PVA in deionized (DI) water) and homogenized at 6000 rpm for 1 min. The PVA solution was made by measuring 15 g PVA, filling to 100 mL with DI water, and mixing in a round bottom flask at 85ºC for 3 h using a condenser. After homogenization, the PDMS-PVA emulsion was heated at 80ºC for at least 3 h on a stir plate at 300 rpm. The solution was diluted to 50 mL with 1 wt.% Pluronic F108 and centrifuged at 3,000x*g* for 10 min. The supernatant containing the small particle size fraction was discarded, and the pellet containing the large fraction was resuspended to the desired concentration in 1 wt.% Pluronic F108 to prevent sticking of particles.

High crosslink density silicone (HCDS) particles for encapsulating palbociclib were synthesized using a nucleation and growth technique [22]. TMOS and DMODMS in a 1:8, 1:12, or 1:16 molar ratio were stirred in a solution of water and 219.5 µL 0.1 M HCl (pH = 2.7) at 500 rpm for 1.5 h to hydrolyze the monomers. The solution was then centrifuged at 2000x*g* for 5 min and the top 7.5 mL extracted for use, leaving behind oligomers, and retaining mostly monomers or dimers. Added to the hydrolyzed monomers were 7.5 mL 3.1 $\times$ 10^{-4} M HCl (pH = 3.5) and 500 µL 2 mg palbociclib / mL DMSO, stirred at 500 rpm for 1 min. Finally, 15 µL of the base catalyst, TEA, was added, and the solution continued to stir at 500 rpm for 30 min while particles grew by polycondensation. After the reaction was complete, the solution was stabilized with 5 mL of 1% w/v Pluronic F108 in DI water.

Resiquimod content in the cured PDMS particles was determined using the previously described solvent release method (Fig. S1) [23]. Briefly, particles were agitated by vortexing in absolute ethanol and centrifuged at 20,000x*g* for 2 min. The supernatant was collected and particles were resuspended in fresh ethanol, followed by additional cycles of agitation, centrifugation, and washing until no detectable amount of drug remained. Supernatant was collected and measured using a UV–vis spectrometer (Tecan Infinite 200) against a calibration curve to quantify the released drug. Palbociclib loading was measured using the same method with 5 vol.% DMSO in water, due to its poor solubility in ethanol.

FIJI (ImageJ2) was used to measure particle size via Otsu's method for thresholding representative micrographs to a sufficiently high number of particles analyzed (n>10,000). A hemocytometer was used to measure particle concentration. SEM was performed in secondary electron imaging mode with high vacuum, at an accelerating voltage of 15,000 V (Hitachi SU3500). Images were taken of particles washed thrice in water to remove Pluronic F108 and any unbound monomers, deposited onto a clean silicon wafer, and coated in 10 nm platinum using a sputter coater (Cressington 108auto).

2.3. Hydrogel synthesis and characterization

In order, 1.25 g acrylamide monomer, 62.5 mg tannic acid, 125 mg ammonium persulfate, 15 µL TEMED, 15 mg *N,N'*-methylenebis(acrylamide), 125 mg glucose, and 0.15 mL particles in DI water at the desired concentration were added to 6.75 mL water heated to 30 °C and stirred at 300 rpm. All components were mixed for 1.5 min and deposited in petri dishes or well plates with a pipette for curing. Hydrogels were sterilized for biological applications through a two-hour UV light exposure in a biosafety cabinet (Thermo Scientific) after complete polymerization.

Tensile adhesion tests of hydrogels attached to dehaired ICR murine skin were performed using a universal testing machine (MTS Exceed Series 40 Electromechanical Universal Test Machine) using a 50 N load cell and loading rate of 0.083 mm/s. Glass slides were glued on either side of the skin and hydrogel (Fig. S2), as previously described [24]. Hydrogels of size 20 mm x 12.5 mm were formed in molds and attached to murine skin soaked in PBS for 24 h to prevent drying. The shear modulus was found from the slope of stress-strain curves generated by tensile tests performed on hydrogels formed in dog bone shaped molds according to American Society for Testing and Materials (ASTM) standard D638–14. A loading rate of 0.5 mm/s was applied until the hydrogels underwent fracture.

Rheological parameters were determined by performing a strain sweep (0.1 – 25%, 1 Hz) and a frequency sweep (0.1 – 50 Hz, 5% strain) on fully polymerized hydrogels without particles at 37 °C. Polymerization kinetics were measured using an 20 mm parallel

plate rheometer (ARES-G2, TA Instruments) at 1 Hz, 5% strain, and a gap height of 1.8 mm for a 60-minute time sweep at 37 °C while the hydrogels formed in situ with mineral oil. Storage and loss moduli were determined from the in situ formed hydrogels following complete polymerization. Each test was performed in triplicate with and without particles. The large fraction of 1:10 LCDS particles (average size = 8.1 μm) was added to the hydrogels at 10×10^6 particles / mL hydrogel precursor for comparing viscoelastic properties, as the large fraction of LCDS particles was expected to have a greater impact on network formation than the smaller HCDS particles.

2.4. Cell culture

RAW 264.7 macrophages were cultured at 37 °C and 5% CO_2 in DMEM supplemented with 10 vol.% heat-inactivated FBS and 1 vol.% penicillin-streptomycin. Tumor-conditioned media (TCM) for culturing RAW 264.7 cells in phenotyping studies was sourced from B16-F10 cells during passaging. No cell line was used beyond passage 15.

2.5. Murine skin explant culture

Skin explants were taken from freshly euthanized female ICR (albino) mice. After removal of the dorsal skin with scissors in aseptic conditions, hair was trimmed with scissors, then the surface was coated with a thin layer of hair removal cream and wiped off using a damp paper towel after 3 min. The stratum corneum was removed by 10 cycles of tape stripping with cellophane [25]. Six mm biopsy punches were collected from across the dorsal skin and placed dermis-side down in a 24-well plate for 15 min or until adherent. Biopsy punches were semi-submerged in 0.2 mL mKer media for culture, as previously described [26]. If a biopsy punch detached, it was moved to a new well and allowed to adhere for 30 more minutes before adding back in media. mKer media was made with 500 mL low glucose DMEM, 167 mL Ham's F12 nutrient mixture, 67 mL heat-inactivated FBS, 5 μg insulin / mL media, 5 μg transferrin / mL media, 0.987 ng 3,3–5′ triiodo-L-thyroxine / mL media, 0.4 μg hydrocortisone / mL media, 10 ng epidermal growth factor / mL media, 60 μg penicillin / mL media, and 25 μg gentamicin / mL media. Components were mixed and passed through a 0.2 μm sterile filter. Media was exchanged for biopsy punches in culture after 24 h.

2.6. Drug release

Drug release studies from particles were performed in 5 vol.% DMSO in PBS or complete DMEM. LCDS particles were synthesized as previously described (see Section 2.2) and aliquots were flushed with absolute ethanol and agitated with vigorous vortexing to measure drug concentration per number of particles. The volume of stock particles used for release of resiquimod was chosen by aliquoting an amount corresponding to 15 μg total drug encapsulated. HCDS particles were synthesized as previously described (see Section 2.2) and aliquots were flushed with 5 vol.% DMSO and agitated with vigorous vortexing to measure drug concentration per number of particles. At specific time points, particles were centrifuged at 5,000xg and an aliquot of solvent was withdrawn for measurement. The remaining supernatant was discarded and replaced. Cumulative release of drug into 5 vol.% DMSO was measured by analyzing the collected supernatants with UV–vis at 320 nm and 353 nm for resiquimod and palbociclib, respectively, in a UV-transparent 96-well plate (Corning). Cumulative release of resiquimod into DMEM was measured by ultraviolet ultra-performance liquid chromatography (UV-UPLC), described in the Supplemental Materials.

For drug release from particles embedded within hydrogels, hydrogels were incubated with cells in a 24-well plate. Hydrogels were formed around inverted P1000 pipet tips in 24-well plates to form donut shapes. After complete polymerization, hydrogels were sterilized using a 2-hour UV light cycle before addition to wells in a fresh 24-well plate. Hydrogels were stuck to the sides of the wells, partially submerged in media, to enable drug release and media exchange but avoid contact with the adherent cell layer. Resiquimod release studies were performed with RAW 264.7 cells to evaluate macrophage polarization.

For skin explant studies, hydrogels were formed in 96-well plates with a volume of 200 uL hydrogel precursor per well. After complete polymerization and sterilization using a 2-hour UV light cycle, hydrogels were removed from the well plate and added to the surface of semi-submerged skin explants biopsy punches in culture. After addition of the hydrogels, media was exchanged after 24 h, and after 48 h, biopsy punches were removed, dissociated, and phenotyped.

2.7. Cell phenotyping

RAW 264.7 cells were collected from well plates and stained with either anti-CD86, anti-CD206, and anti-MHCII antibodies or permeabilized and stained with anti-iNOS and anti-Arg-1 antibodies. Complete methods can be found in the Supplementary Materials.

2.8. Tissue dissociation and phenotyping

Skin biopsy punches were removed from culture, minced into 1 mm pieces with a scalpel (without mashing), and placed into 1 mL Accumax digestion solution in a 24-well plate. The plate was incubated at 37 °C for 25 min with orbital shaking. The solutions were transferred into a 40 μm cell strainer and pushed through with a syringe plunger for several minutes, with periodic rinsing with PBS. Material stuck in the filter was disposed, and the collected material was centrifuged at 350xg for 10 min at 4 °C. The pellet was resuspended in stain buffer and cells counted (to ensure no group exceeded 10^8 cells), and reagents for $CD45^+$ cell selection from an EasySep (Stem Cell) kit were added according to instructions from the manufacturer. Each sample underwent two rounds of magnetic separation, after which point, $CD45^+$ cells were counted (to ensure no group exceeded 10^6 cells) and stained as described in the Supplementary Materials with the addition of anti-CD11b and anti-F4/80 surface staining antibodies to identify macrophages. The gating scheme for different immune cell populations is shown in the Supplementary Materials (Fig. S3).

2.9. Statistical analysis

Data in Fig. 2 are shown as mean ± standard deviation (SD). Data in Fig. 3 and Fig. 4 are shown as median fluorescence ± standard error (SE). For determination of statistical significance, multiple unpaired, equal variance t-tests were used, as applicable. Significance was determined at the cutoff point $^*P < 0.05$.

3. Results

3.1. Hydrogel synthesis and adhesion

We chose a polyacrylamide (PAM) backbone for this hydrogel system, due to its common use as a polymer in biological applications, biocompatibility, strong resistance to degradation, and amenability to modification for incorporating adhesive groups [27]. Further, PAM toughness, as measured by fracture energy, is commensurate with human skin [2], making it an ideal material for

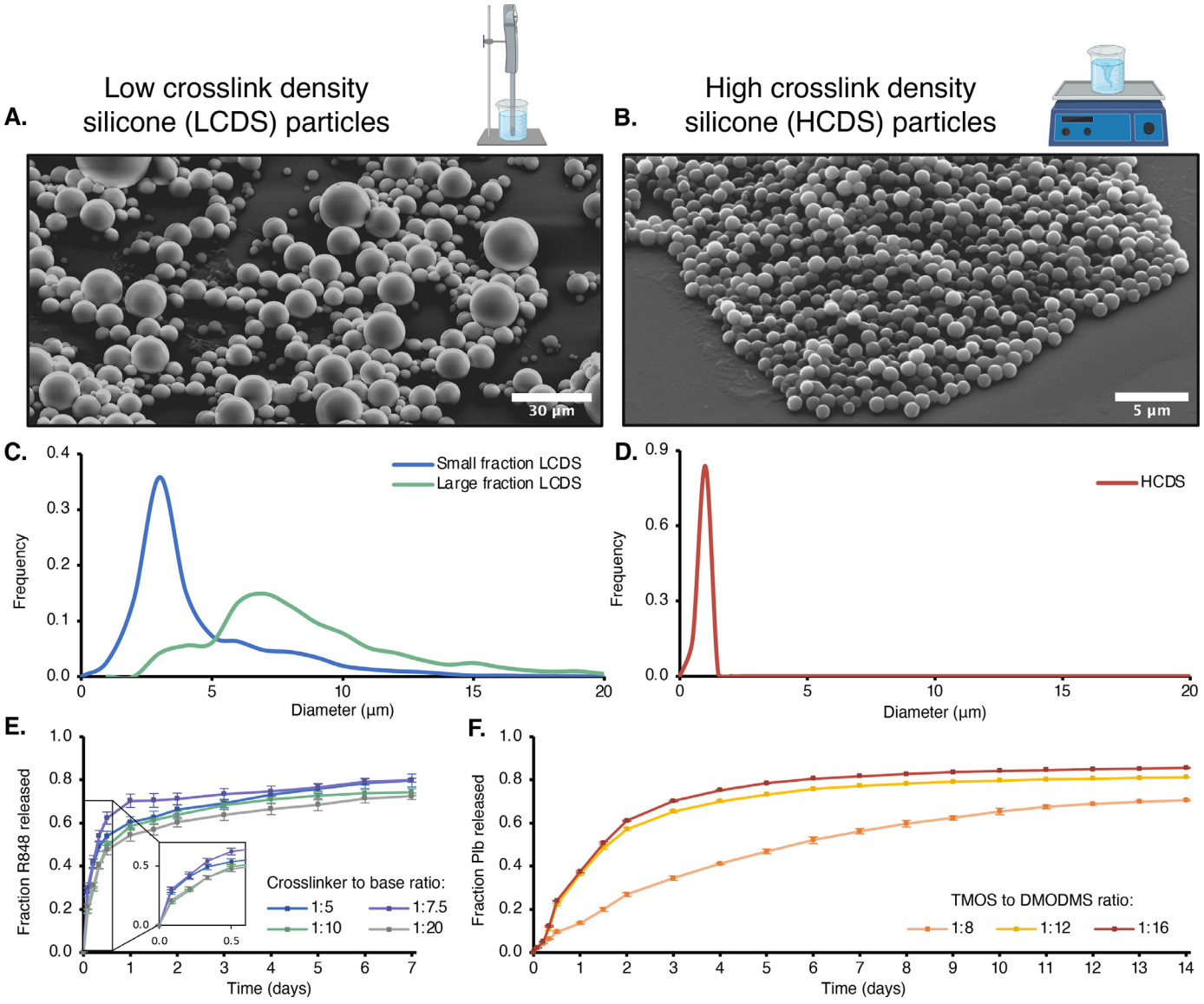

Fig. 2. Particle characterization and drug release. A) Large size fraction of LCDS particles, synthesized using homogenization and separated by differential centrifugation, imaged with scanning electron microscopy (SEM). B) HCDS particles, synthesized using a nucleation and growth technique, imaged with SEM. C) Size distribution of resiquimod-containing LCDS particles made from different ratios of crosslinker to base, split into small and large fractions (N = 11,000 particles). D) Size distribution of palbociclib-containing HCDS particles made from different ratios of TMOS to DMODMS (N = 23,000 particles). E) Rapid release of resiquimod over one week from particles with varied crosslinking density (1:5, 1:7.5, 1:10, and 1:20 crosslinker to base; N = 5). F) Slow release of palbociclib over two weeks from particles made from 1:8, 1:12, and 1:16 molar ratios of TMOS to DMODMS (N = 5).

transdermal applications. Synthesis occurs by way of free radical vinyl addition polymerization of acrylamide monomers to form PAM. Additional functionalization with galloyl groups, found in the polyphenol tannic acid, imparts adhesive capabilities to the hydrogel by binding to proteins in the skin [28]. A universal testing machine was used for tensile-adhesion tests to pull the hydrogel from dehaired murine skin explants. The hydrogel showed an average adhesive strength of 1348 ± 211 Pa (N = 5, Fig. S2). Higher adhesiveness can be achieved without affecting drug release rate by varying the content of galloyl groups or water in the hydrogel and testing on more physiologically relevant models such as porcine or human skin. Furthermore, adhesion mediated by polyphenols has been shown to increase in strength with contact time (i.e., up to 24 h), while these hydrogels were only in contact with murine skin for five minutes to avoid loss of moisture in the skin explants [29].

Hydrogel mesh size was also approximated from tensile testing data to ensure that drug release kinetics were not affected by the hydrogel network (Fig. S4). Using the classical theory of rubber elasticity, shear modulus (G) is related to hydrogel mesh size (r_{mesh}) by the equation:

$$r_{mesh} = \left(\frac{6RT}{\pi N_{Av} G}\right)^{1/3}$$

where R is the gas constant, T is the absolute temperature, and N_{Av} is Avogadro's number [4]. Calculating shear modulus from the stress-strain curve yields a mesh size of 17.9 ± 1.5 nm (N = 6), which is substantially larger than the diameter of small molecule drugs such as palbociclib and resiquimod [30], which will allow free passage of the drugs once released from the particles.

3.2. Particle synthesis and drug loading

To achieve multimodal drug release, two types of silicone particles were synthesized and embedded into the hydrogel (Fig. 2)

[22,31]. While the mesh size of the hydrogel can also affect the kinetics of drug release [4], we selected a sufficiently large mesh size such that the kinetics were fully decoupled from hydrogel network properties and solely dependent on the particle formulation. To enable the rapid release of resiquimod (i.e., 50% release in one day), we prepared low crosslink density silicone (LCDS) particles using a commercial PDMS kit (Sylgard 184) (Fig. 2A). The standard 1:10 ratio of crosslinker to base results in a mesh diameter ranging from 4 to 35 nm [31]. We therefore evaluated the LCDS particles synthesized with crosslinker to base ratios from 1:5 to 1:20 to determine the effect on resiquimod release. To encapsulate resiquimod, the PDMS precursor was mixed with resiquimod dissolved in a small volume of DMSO prior to homogenization in an aqueous solvent. Particles made using this approach had an average resiquimod encapsulation efficiency of 7.5 ± 1.1% across all conditions. The low drug loading efficiency was likely due to the relatively large mesh size of the PDMS. Drug loading was measured by a solvent release assay described elsewhere [23], where particles are flushed multiple times with a favorable solvent (i.e., ethanol) to extract encapsulated drug for measurement using a calibration curve. This method leads to a more conservative estimation of drug loading than measuring the supernatant after particle synthesis because potential sources of drug loss (e.g., drug trapped on the stir bar, adsorbed to the walls of the container) are accounted for (Fig. S1). To reduce particle polydispersity, a 15 wt.% PVA solution was used as the aqueous phase during homogenization, resulting in an average particle size of 6.5 ± 9.1 μm and a coefficient of variance (CV) of 1.4 (Fig. 2C, Fig. S5). Particle size was further refined by differential centrifugation, resulting in two subpopulations, the larger size of which (mean = 8.1 ± 11.1 μm, CV = 1.4) was used due to its ability to readily pellet.

To enable slow release of palbociclib (i.e., 50% release in five days), high crosslink density silicone (HCDS) particles were synthesized using a one-pot nucleation and growth technique (Fig. 2B) [23]. Here, particle mesh size is controlled by the relative abundance of alkoxide groups present in alkoxysilane and silicon alkoxide monomers used in the reaction. We varied the ratio of tetrafunctional monomers (tetramethoxysilane, TMOS) to difunctional monomers (dimethoxydimethylsilane, DMODMS), which can form up to four or two siloxane bonds after polycondensation, respectively, with an alkaline catalyst. A denser mesh (i.e., due to a higher ratio of TMOS to DMODMS) resulted in slower drug release [23]. Therefore, we evaluated particles made with 1:8, 1:12, and 1:16 molar ratios of TMOS to DMODMS to achieve slow release of palbociclib. To encapsulate drug within the particles, palbociclib dissolved in a small volume of DMSO was added at the beginning of the polycondensation step, resulting in an average loading efficiency of 93.6 ± 7.7% across all particle conditions. While ethanol could not be used for the solvent release assay to determine drug loading in the HCDS particles due to its relatively low density, 5 vol.% DMSO was used with agitation to collect all encapsulated drug prior to release kinetics experiments. HCDS particles had a narrower size distribution than the LCDS particles, resulting in an average size of 0.67 ± 0.17 μm and a CV of 0.26 (Fig. 2D, Fig. S5).

3.3. Drug release from particles

To identify the appropriate formulation (i.e., crosslink density) of each type of particle, we performed a series of controlled release studies. Fast-releasing LCDS particles were made to encapsulate resiquimod and stimulate macrophages. Slow-releasing HCDS particles were made to encapsulate palbociclib and stimulate T cells. Immediately following synthesis, both types of particles were suspended in 5 vol.% DMSO in PBS to facilitate drug release. LCDS particles released 50% of their payload within 24 h, with more gradual release over the rest of a week in all crosslinker conditions (Fig. 2E). Therefore, the standard ratio of 1:10 crosslinker to base was selected for all subsequent experiments. We also studied the release of resiquimod from LCDS particles (1:10 crosslinker to base) in complete cell media. Due to the high levels of resiquimod released (i.e., above the linear region of the standard curve), the UV-UPLC detector was overloaded. Thus, while the exact concentrations were not identified, we were able to map the trend of resiquimod release by extrapolating the average amount of drug release from Days 1–5. We then approximated the complete release of drug to calculate fractional release and found similar release kinetics in both solvents over a period of five days (Fig. S6). This finding confirms that the release experiments performed in 5 vol.% DMSO (shown in Fig. 2) are a reasonable model for drug release in complete cell media.

In contrast to the LCDS particles, the release rate of drug from HCDS particles was highly dependent on crosslink density; in particular, the 1:8 TMOS to DMODMS particle condition released less than 15% of its encapsulated payload in 24 h and only 70% over two weeks (Fig. 2F). The 1:12 and 1:16 conditions had similar release profiles, both of which achieved over 35% release within 24 h and leveled off.

3.4. Hydrogel polymerization kinetics

Using in situ rheological analysis, we identified a hydrogel formulation that polymerizes rapidly (90% gelation within 20 min after the addition of crosslinker at 37 °C) and displays a storage modulus of 90.5 kPa and a loss modulus of 0.41 kPa (Fig. S7). However, we hypothesized that both gelation kinetics and storage modulus would be affected by the concentration of particles added to the hydrogel precursors due to obstruction of network formation. Thus, we evaluated the upper limit of particles that could be added to the hydrogel while maintaining rapid polymerization kinetics (Fig. S7). For this study, we used LCDS particles with an average size of 8.1 ± 11.1 μm (Fig. 2B). Our analysis revealed that a hydrogel will still form with a storage modulus of 1.5 kPa and loss modulus of 8.5 Pa with up to 10×10^6 particles / mL hydrogel precursor. Also, there was no significant difference in the rate of polymerization whether particles were present in the hydrogel or not (near complete polymerization occurred after 30 min). The sol-gel transition kinetics of hydrogels both with and without particles is consistent with data and curve fitting found in literature [32].

3.5. Immune cell activation in vitro

The complete hydrogel system containing resiquimod was next tested *in vitro* to stimulate RAW 264.7 murine macrophages cultured in 10 vol.% TCM. Hydrogels were formed into “donut” shapes with the outer diameter 3x the inner diameter, matching the width of a 24-well plate well. Their donut geometry and ability to adhere to surfaces allowed the hydrogels to be suspended, partially submerged, in a 24-well plate by sticking to the walls. Therefore, drug was released from LCDS particles into the media without disturbing the cell layer, while permitting gas and media exchange through the center of the hydrogel. Cell polarization was measured via flow cytometry on Days 1 and 5 of culture and normalized to cells cultured with an empty hydrogel (i.e., the hydrogel vehicle without any drug). We examined the expression of markers associated with macrophage polarization to compare the durability of phenotypic changes caused by the release of resiquimod from the hydrogel system to that of a single bolus injection, representative of current methods of drug administration. Free resiquimod was added to the wells to produce a concentration of 150 nM. In contrast, release of resiquimod from the hydrogel was estimated to be 70.5 nM after Day 1 based on data shown in Fig. 2. Cell media was exchanged in all conditions after 24 and 72 h to simulate a

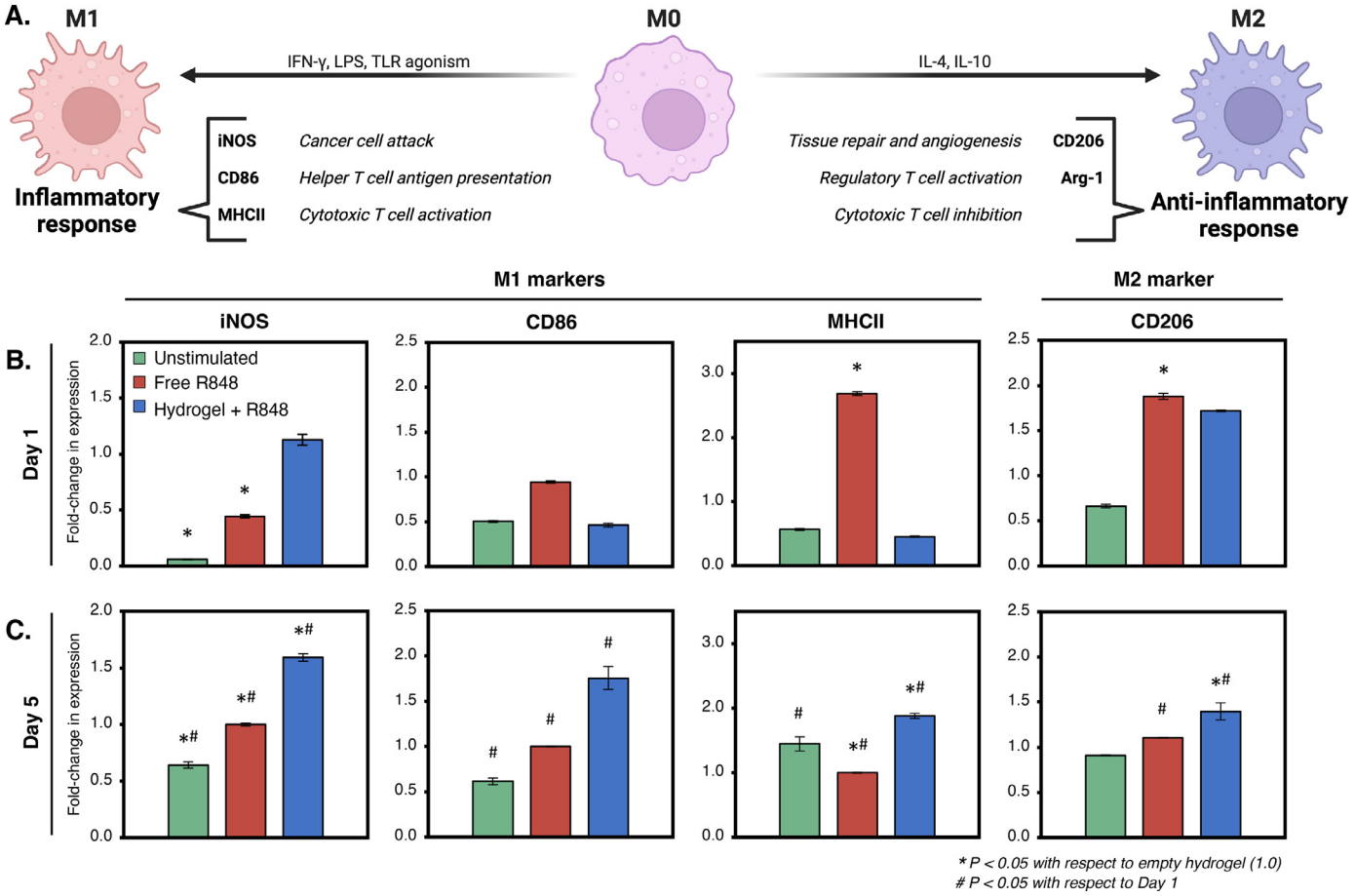

Fig. 3. Macrophage modulation by resiquimod release from hydrogels *in vitro*. A) Schematic illustration of macrophage phenotypes in response to pro-inflammatory or anti-inflammatory signals. Relative expression of M1-associated markers (iNOS, MHCII, and CD86) and an M2-associated marker (CD206) on murine macrophages, relative to that of control cells incubated with an empty hydrogel vehicle after B) one and C) five days in culture in 10 vol.% TCM ($N = 3$, $P<0.05$).

physiological sink for the drug (e.g., due to absorption, diffusion, or metabolism) (Fig. 3A,B). All fold-changes in marker expression are relative to cells incubated with an empty hydrogel to account for potential stimulatory effects of the hydrogel. Markers examined include inducible nitric oxide synthase (iNOS), arginase-1 (Arg-1), cluster of differentiation 86 (CD86), major histocompatibility complex class II (MHCII), and CD206. iNOS controls the production of nitric oxide, a cytotoxic and tumoricidal agent, and is strongly upregulated by inflammatory cytokines (e.g., interferon gamma, IFN-γ), making it a common biomarker for M1 macrophage phenotypes. Conversely, Arg-1 production can inhibit iNOS and suppress M1 phenotypes [33]. MHCII and CD86 play roles in adaptive immunity as an antigen-presenter to T helper cells and a costimulatory molecule for antigen presentation, respectively [34]. Thus, MHCII and CD86 are overexpressed on M1 macrophages. Finally, CD206 is a mannose receptor associated with protumoral behaviors such as clearance of inflammatory proteins and profibrotic effects by fibroblast growth, indicative of M2 polarizations [35]. While there was a minor increase in the expression of all markers in the condition of the empty hydrogel compared to the unstimulated cells (i.e., negative control), this effect did not surpass the intended effect caused by resiquimod by a significant amount in any case.

In macrophages receiving free resiquimod, we observed a temporary increase in expression of MHCII and CD86 (M1 markers) on Day 1, while all markers returned near to levels associated with the empty hydrogel control by Day 5. In all cases, the free resiquimod conditions had M1 markers elevated over the unstimulated cells, indicating sufficient TLR7/8 stimulation at 150 nM. However, the decrease in marker expression, nearly to 1.0 (i.e., equivalent expression to the empty hydrogel) by Day 5, indicates that macrophages polarized toward M1 phenotypes will lose their phenotype without additional stimulation. On the other hand, resiquimod release from hydrogels containing LCDS particles caused an increase in M1-associated biomarker expression from Day 1 to Day 5 in all cases and a decrease in M2 marker expression. Arg-1 had no significant response and therefore is not shown here.

3.6. *Immune cell activation* ex vivo

To validate our *in vitro* data, we studied the release of resiquimod from the hydrogel system when attached to murine skin explants from freshly euthanized mice. Skin was removed, dehaired, and tape-stripped to remove the stratum corneum and allow for transdermal penetration of drugs. Prior to applying the hydrogel, we validated the penetration of resiquimod into murine skin through the use of a surrogate hydrophobic small molecule fluorescent dye, BODIPY FL C_5 (molecular weight = 320 Da) [36]. After 24 h, the dye permeated 370 ± 126 µm, demonstrating that tissue-resident immune cells can be stimulated by topical release of drug after one day (Fig. S8).

Processed skin was biopsied and added to culture media with a cylindrical hydrogel of the same diameter adhered to the top surface. The biopsy punches were partially submerged in media to facilitate adhesion of the hydrogel to the tissue, incubated for two days, and dissociated for phenotyping (Fig. 4A). Macrophages were identified as $CD45^+$, $CD11b^+$, and $F4/80^+$ cells, and a subset of

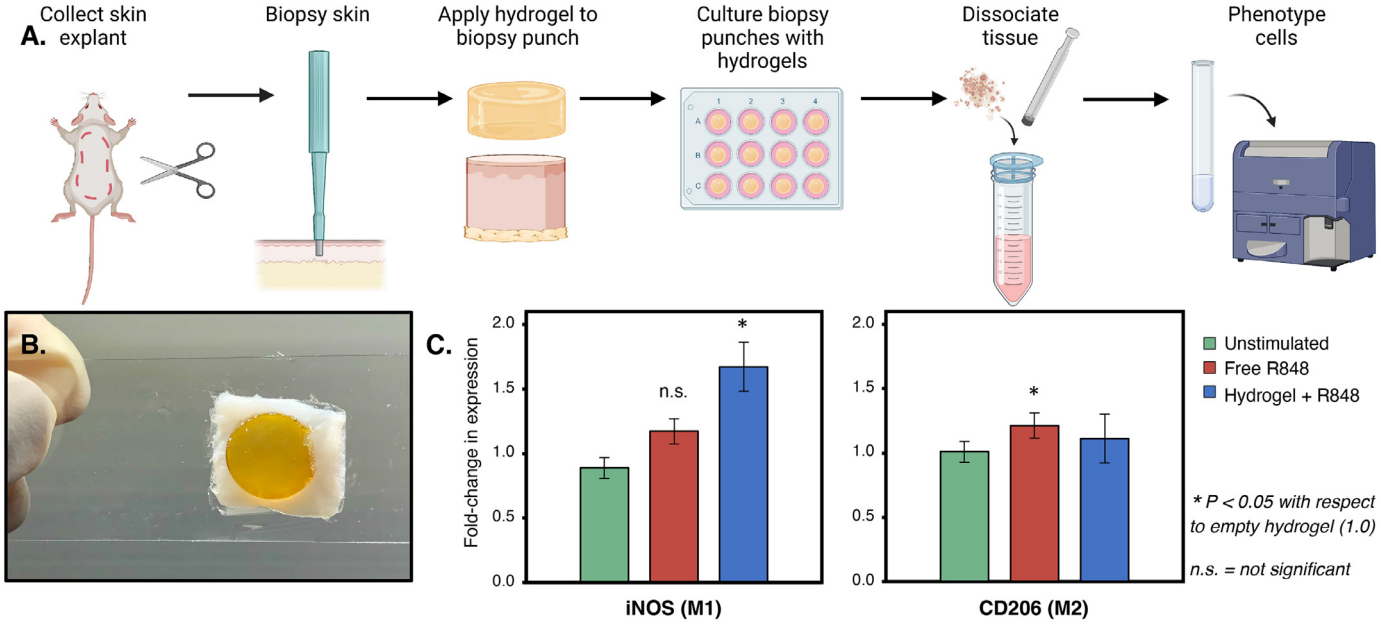

Fig. 4. Macrophage modulation by resiquimod release from hydrogels *ex vivo*. A) Graphical illustration of skin explant collection, preparation, and dissociation. B) Example of adhesion between a hydrogel and murine skin on a glass slide. Dimensions not reflective of biopsy punches and hydrogels in culture. C) M1-associated marker iNOS and M2-associated marker CD206 expression on primary murine macrophages after two days of culture without stimulation, with free resiquimod, or with a resiquimod-containing hydrogel, relative to that of macrophages from biopsied skin adhered to an empty hydrogel vehicle ($N = 3$, $P<0.05$).

leukocytes was permeabilized for analysis of intracellular marker expression (Fig. S3). Free resiquimod was added to the culture media to a concentration of 250 nM, and the hydrogels were estimated to release 250 nM resiquimod by Day 1 from the embedded LCDS particles based on data shown in Fig. 2 and Figure S6. Concentrations were increased from the RAW 264.7 cell experiments to account for transport through the tissue.

Primary cells from the cultured skin explants had a significant increase in iNOS expression due to incubation with the hydrogel system, whereas the relative change in expression due to free resiquimod was not significant compared to the empty hydrogel control. This result is consistent with our *in vitro* studies and confirms that the slow release of resiquimod from the hydrogel system has the capacity to promote durable immune responses. However, the M2 marker CD206 increased significantly in response to the addition of free resiquimod, whereas there was no significant increase observed in the resiquimod-containing hydrogel condition. The M2-associated marker Arg-1 and M1-associated markers CD86 and MHCII were also examined, with no significant changes identified in any condition. Furthermore, we did not observe a significant reduction in cell viability when explants were cultured with hydrogels; the unstimulated control contained 96.3 ± 0.6% viable single cells after dissociation, and the empty hydrogel contained 92.4 ± 5.7%. As the murine skin explants are most representative of the physiological application of this hydrogel system, these results indicate a lack of toxicity from the hydrogel. Finally, there is no significant difference between marker expression in the control condition and the empty hydrogel, indicating a lack of inflammatory response caused by hydrogel attachment. Removal of the hydrogel system after 1–2 weeks of application will also avoid long term effects on the skin.

4. Discussion

We demonstrate the design and implementation of a tunable hydrogel system with drug release properties that are decoupled from those of the hydrogel vehicle. The polymer backbone, PAM, is functionalized with galloyl groups to achieve tissue adhesion. Similar phenol groups, catechols, are found in the muscle foot protein [37] and on the poison ivy toxin [38,39], enabling stable attachment for days to weeks. This adhesive chemistry has been exploited by a number of hydrogels with applications ranging from wound healing to cellular therapy [2,40–42], and tissue adhesion mediated by tannic acid has also been shown to achieve strong underwater adhesion, supporting the feasibility of this hydrogel system to tolerate daily wear [43]. Furthermore, we found that the storage and loss moduli, but not polymerization kinetics, are affected by particle loading when large LCDS particles were embedded at a high concentration. These effects can be reduced by using smaller particles or lower particle concentrations. However, the minimal difference in polymerization rate when hydrogels were formed with or without particles demonstrates how this hydrogel system can be easily deposited into various sites (e.g., those formed by microneedle rolling or surgical resection). This consistency is useful for most topical applications, as hydrogels must polymerize predictably within a reasonable time frame (e.g., <30 min). Furthermore, these results indicate that a high upper limit of particles, and thus drug, can be loaded into the hydrogel while polymerizing reliably. In the complete hydrogel system, the total amount of drug loaded can be varied by i) drug concentration encapsulated in the particles, ii) particle density within the hydrogel, and/or iii) volume of the hydrogel applied to the skin. Therefore, appropriate dosing of individual drug types can be controlled by multiple means. As the LCDS particles have a lower drug encapsulation efficiency than the HCDS particles, they are the limiting variable for drug loading. Using the maximum particle encapsulation concentration for LCDS particles found via rheology (Fig. S7), we estimate that ~9 ng of drug can be contained per mm^3 of hydrogel. To assess whether this maximal loading will affect downstream applications, we consider a melanoma resection site as an example deployment location for our hydrogel. For moderately sized melanoma resections (i.e., 6 mm tumor diameter, 1 mm margin, 1 mm depth, according to the National Comprehensive Cancer Network), this loading would equate to a concentration of 18.4 μM of resiquimod delivered to a volume of the same size directly below the hydrogel, far surpassing the half-maximal

effective concentration (EC_{50}) of 14.1 nM necessary for cell activation [16]. For applications requiring a higher drug loading capacity, other types of particles that confer higher encapsulation efficiencies can be used (e.g., 1:16 TMOS to DMODMS HCDS particles).

Multimodal drug release was demonstrated by preparing silicone particles with different crosslink densities. Release of resiquimod from the LCDS particles into solvent was near-linear within the first 12 h, likely due to drug release near the surface of the particles, which is consistent with standard models of small molecule drug diffusion out of a spherical polymer matrix [44]. Slower diffusion through the network dominated after the first day. The negligible difference in release rate across crosslinker to base conditions suggests that resiquimod had free passage out of the LCDS particles at all crosslink densities, indicating that even a high crosslink density of PDMS results in a sufficiently large mesh size for rapid release of resiquimod (i.e., drug size << mesh size). Therefore, tuning drug release rate from the LCDS particles would rely on properties other than crosslink density such as particle size (i.e., surface area to volume ratio) and drug size. On the other hand, palbociclib release from HCDS particles was inhibited, resulting in more sustained release, suggesting that the drug size was closer to the particle mesh size in all conditions. Although mesh size does not appear to change linearly with TMOS:DMODMS, as seen by the similar release kinetics of 1:12 and 1:16 conditions, other ratios of TMOS to DMODMS may allow for finer control over the release rate of palbociclib and other small molecule drugs to achieve the desired kinetics for different applications. However, we note that a 1:4 ratio of TMOS:DMODMS did not form well-defined particles using the methods described here.

Controlled release of drugs from microparticles embedded within the hydrogel resulted in sustained cell activation *in vitro* and *ex vivo* compared to controls. When tracking resiquimod release from hydrogels over time *in vitro*, cellular biomarkers evaluated include iNOS, MHCII, CD86, and CD206. Resiquimod release from hydrogels containing LCDS particles resulted in higher expression of all markers by Day 5. This more durable response is likely due to the rapid release of resiquimod in the first 24 h causing initial activation, followed by slower but sustained release across the subsequent days that maintained cellular phenotypes. We expect that a similar trend would occur *ex vivo* if examined over a longer period, although there was still positive activity after two days. We show that a surrogate for resiquimod can penetrate skin *ex vivo*370 $\pm$ 126 µm after 24 h (Fig. S8), yielding a speed of 15.4 $\pm$ 5.3 µm/hour, therefore demonstrating that any cellular activation is due to release of drug. Topical drug penetration has also been shown *in vivo* with similar results [36]. The relative expression of iNOS was highest in the explant group treated with the hydrogels containing LCDS particles. This result was significant compared to the control condition of free resiquimod over the same two-day duration, demonstrating that the slow release of drugs from the hydrogel resulted in more durable immune responses. M1-activated macrophages release proinflammatory factors such as cytokines and nitric oxide, potentiating an inflammatory response after drug stimulation; therefore, sustained TLR7/8 agonism by resiquimod may result in an elevated inflammatory response when compared to a bolus addition of drug. Furthermore, the relative expression of CD206 was not significantly different between the hydrogel group and the unstimulated control, indicating no M2 marker upregulation.

5. Conclusion

We have demonstrated the preparation and use of a hydrogel system that can attach to skin and controllably release drugs in a manner that is fully decoupled from the bulk properties of the hydrogel. We show that by using multiple types of silicone particles, these hydrogels enable multimodal release of drugs that have the capacity to independently stimulate multiple cell types for a robust and sustained therapeutic effect. The tunable nature of this hydrogel offers the potential to address a variety of topical uses and advance dermatological capabilities. For instance, this hydrogel system could be used for transdermal vaccine delivery by co-encapsulating adjuvant- and antigen-containing particles [45]. This could be accomplished by treating the surfaces of particles with adhesive coatings such as a metal-phenolic network or using particles made from alternative polymers to encapsulate biologics [46]. Such hydrogels can be applied to surgical resection sites—following the current standard-of-care for most skin carcinomas—or deposited using microneedles [47–49]. Skin perforations can be created using the “poke and patch” microneedle rolling technique immediately followed by application of the hydrogel [50,51]. While we focused on regulating the phenotypes of immune cells, this hydrogel can be adapted to target a variety of cell populations for the purposes of treating skin cancers, wounds, and autoimmune disorders. Overall, this modular and programmable hydrogel system provides a simple means by which the safety and efficacy of drugs delivered to the skin can be enhanced.

Declaration of Competing Interest

There are no conflicts of interest to declare.

Acknowledgements

The authors thanks Dr. Jin G. Lee for assistance with collecting SEM images, Dr. Christopher Ebmeier in the Mass Spectrometry Facility for assistance developing and running the resiquimod detection assay, and Dr. Joseph Dragavon in the Advanced Light Microscopy core for advising the skin penetration study. The authors also thank Dr. Junling Guo of the BMI Center at Sichuan University for helpful discussions. This work was supported by the NIH/CU Molecular Biophysics Program and NIH Biophysics Training Grant T32 GM-065103 and the Teets Family Endowed Doctoral Fellowship in Nanotechnology. The authors also acknowledge support from the Mass Spectrometry Core, the BioFrontiers Institute Advanced Light Microscopy Core (RRID: SCR_018302), the Colorado Shared Instrumentation in Nanofabrication and Characterization (RRID: SCR_018985), and the Flow Cytometry Shared Core (S10ODO21601) at the University of Colorado Boulder. The Nikon Ti-E Widefield is supported by NIH grant R01CA107098S1. Some of the figures in this article were made using BioRender.com.

Supplementary materials

Supplementary material associated with this article can be found, in the online version, at doi:10.1016/j.actbio.2022.07.053.

References

[1] C.W. Shields, L.L.W. Wang, M.A. Evans, S. Mitragotri, Materials for Immunotherapy, Adv. Mater. 1901633 (2019) 1–56, doi:10.1002/adma.201901633.
[2] L. Han, L. Yan, K. Wang, L. Fang, H. Zhang, Y. Tang, Y. Ding, L.T. Weng, J. Xu, J. Weng, Y. Liu, F. Ren, X. Lu, Tough, self-healable and tissue-adhesive hydrogel with tunable multifunctionality, NPG Asia Mater 9 (2017), doi:10.1038/am.2017.33.
[3] A.S. Hoffman, Hydrogels for biomedical applications, Adv. Drug Deliv. Rev. 64 (2012) 18–23, doi:10.1016/j.addr.2012.09.010.
[4] J. Li, D.J. Mooney, Designing hydrogels for controlled drug delivery, Nat. Rev. Mater. (2016) 1, doi:10.1038/natrevmats.2016.71.
[5] Y. Tahara, S. Kosuge, S. Sawada, Y. Sasaki, K. Akiyoshi, Nanogel bottom-up gel biomaterials for protein delivery: photopolymerization of an acryloyl-modified polysaccharide nanogel macromonomer, React. Funct. Polym. 73 (2013) 958–964, doi:10.1016/j.reactfunctpolym.2013.02.002.
[6] K. Numata, S. Yamazaki, N. Naga, Biocompatible and biodegradable dual-drug release system based on silk hydrogel containing silk nanoparticles, Biomacromolecules 13 (2012) 1383–1389, doi:10.1021/bm300089a.

[7] B. Song, C. Wu, J. Chang, Dual drug release from electrospun poly(lactic-co-glycolic acid)/mesoporous silica nanoparticles composite mats with distinct release profiles, Acta Biomater 8 (2012) 1901–1907, doi:10.1016/j.actbio.2012.01.020.
[8] J. Wang, M. Windbergs, Controlled dual drug release by coaxial electrospun fibers – Impact of the core fluid on drug encapsulation and release, Int. J. Pharm. 556 (2019) 363–371, doi:10.1016/j.ijpharm.2018.12.026.
[9] M.A. Campea, M.J. Majcher, A. Lofts, T. Hoare, A Review of Design and Fabrication Methods for Nanoparticle Network Hydrogels for Biomedical, Environmental, and Industrial Applications, Adv. Funct. Mater. (2021) 31, doi:10.1002/adfm.202102355.
[10] D.F. Williams, Challenges with the development of biomaterials for sustainable tissue engineering, Front. Bioeng. Biotechnol. 7 (2019) 127, doi:10.3389/fbioe.2019.00127.
[11] M.D. Swartzlander, C.A. Barnes, A.K. Blakney, J.L. Kaar, T.R. Kyriakides, S.J. Bryant, Linking the foreign body response and protein adsorption to PEG-based hydrogels using proteomics, Biomaterials 41 (2015) 26–36, doi:10.1016/j.biomaterials.2014.11.026.
[12] D.S. Kohane, Microparticles and nanoparticles for drug delivery, Biotechnol. Bioeng. 96 (2007) 203–209, doi:10.1002/bit.21301.
[13] Stefan Willhelm, Anthony J. Tavares, Qin Dai, Seiichi Ohta, Julie Audet, Harold F. Dvorak, Warren C.W. Chan, Analysis of nanoparticle delivery to tumours, Nat. Rev. Mater. 1 (2016), doi:10.1038/natrevmats.2016.14.
[14] R. Goyal, L.K. Macri, H.M. Kaplan, J. Kohn, Nanoparticles and nanofibers for topical drug delivery, J. Control. Release. 240 (2016) 77–92, doi:10.1016/j.jconrel.2015.10.049.
[15] C. Raman, C. Berkland, K. Kim, D.W. Pack, Modeling small-molecule release from PLG microspheres: effects of polymer degradation and nonuniform drug distribution, J. Control. Release. 103 (2005) 149–158, doi:10.1016/j.jconrel.2004.11.012.
[16] C.B. Rodell, S.P. Arlauckas, M.F. Cuccarese, C.S. Garris, R. Li, M.S. Ahmed, R.H. Kohler, M.J. Pittet, R. Weissleder, TLR7/8-agonist-loaded nanoparticles promote the polarization of tumour-associated macrophages to enhance cancer immunotherapy, Nat. Biomed. Eng. 2 (2018) 578–588, doi:10.1038/s41551-018-0236-8.
[17] F.O. Martinez, S. Gordon, The M1 and M2 paradigm of macrophage activation: time for reassessment, F1000Prime Rep. 6 (2014) 1–13, doi:10.12703/P6-13.
[18] J. Deng, E.S. Wang, R.W. Jenkins, S. Li, R. Dries, K. Yates, S. Chhabra, W. Huang, H. Liu, A.R. Aref, E. Ivanova, C.P. Paweletz, M. Bowden, C.W. Zhou, G.S. Herter-Sprie, J.A. Sorrentino, J.E. Bisi, P.H. Lizotte, A.A. Merlino, M.M. Quinn, L.E. Bufe, A. Yang, Y. Zhang, H. Zhang, P. Gao, T. Chen, M.E. Cavanaugh, A.J. Rode, E. Haines, P.J. Roberts, J.C. Strum, W.G. Richards, J.H. Lorch, S. Parangi, V. Gunda, G.M. Boland, R. Bueno, S. Palakurthi, G.J. Freeman, J. Ritz, W.Nicholas Haining, N.E. Sharpless, H. Arthanari, G.I. Shapiro, D.A. Barbie, N.S. Gray, K.K. Wong, CDK4/6 inhibition augments antitumor immunity by enhancing T-cell activation, Cancer Discov 8 (2018) 216–233, doi:10.1158/2159-8290.CD-17-0915.
[19] M. Heckler, L.R. Ali, E. Clancy-Thompson, L. Qiang, K.S. Ventre, P. Lenehan, K. Roehle, A. Luoma, K. Boelaars, V. Peters, J. McCreary, T. Boschert, E.S. Wang, S. Suo, F. Marangoni, T.R. Mempel, H.W. Long, K.W. Wucherpfennig, M. Dougan, N.S. Gray, G.C. Yuan, S. Goel, S.M. Tolaney, S.K. Dougan, Inhibition of cdk4/6 promotes cd8 t-cell memory formation, Cancer Discov 11 (2021) 2564–2581, doi:10.1158/2159-8290.CD-20-1540.
[20] M.A. Sallam, S. Prakash, N. Kumbhojkar, C.W. Shields, S. Mitragotri, Formulation-based approaches for dermal delivery of vaccines and therapeutic nucleic acids: recent advances and future perspectives, Bioeng. Transl. Med. 6 (2021) 1–28, doi:10.1002/btm2.10215.
[21] L.M. Johnson, L. Gao, C.W. Shields, M. Smith, K. Efimenko, K. Cushing, J. Genzer, G.P. López, Elastomeric microparticles for acoustic mediated bioseparations, J. Nanobiotechnology. 11 (2013) 1–8, doi:10.1186/1477-3155-11-22.
[22] C.W. Shields, D. Sun, K.A. Johnson, K.A. Duval, A.V. Rodriguez, L. Gao, P.A. Dayton, G.P. López, Nucleation and growth synthesis of siloxane gels to form functional, monodisperse, and acoustically programmable particles, Angew. Chemie Int. Ed. 53 (2014) 8070–8073, doi:10.1002/anie.201402471.
[23] C.W. Shields, J.P. White, E.G. Osta, J. Patel, S. Rajkumar, N. Kirby, J.P. Therrien, S. Zauscher, Encapsulation and controlled release of retinol froma silicone particles for topical delivery, J. Control. Release. 278 (2018) 37–48, doi:10.1016/j.jconrel.2018.03.023.
[24] H. Jung, M.K. Kim, J.Y. Lee, S.W. Choi, J. Kim, Adhesive Hydrogel Patch with Enhanced Strength and Adhesiveness to Skin for Transdermal Drug Delivery, Adv. Funct. Mater. 30 (2020) 1–10, doi:10.1002/adfm.202004407.
[25] M. Takigawa, Y. Tokura, H. Hashizume, H. Yagi, N. Seo, Percutaneous peptide immunization via corneum barrier - Disrupted murine skin for experimental tumor immunoprophylaxis, Ann. N. Y. Acad. Sci. 941 (2001) 139–146, doi:10.1111/j.1749-6632.2001.tb03717.x.
[26] N.S. Tan, W. Wahli, Studying Wound Repair in the Mouse, Curr. Protoc. Mouse Biol. 3 (2013) 171–185, doi:10.1002/9780470942390.mo130135.
[27] M.C. Darnell, J.Y. Sun, M. Mehta, C. Johnson, P.R. Arany, Z. Suo, D.J. Mooney, Performance and biocompatibility of extremely tough alginate/polyacrylamide hydrogels, Biomaterials 34 (2013) 8042–8048, doi:10.1016/j.biomaterials.2013.06.061.
[28] J. Saiz-Poseu, J. Mancebo-Aracil, F. Nador, F. Busqué, D. Ruiz-Molina, The Chemistry behi nd Catechol-Based Adhesion, Angew. Chemie - Int, Ed. 58 (2019) 696–714, doi:10.1002/anie.201801063.
[29] N. Pandey, A. Hakamivala, C. Xu, P. Hariharan, B. Radionov, Z. Huang, J. Liao, L. Tang, P. Zimmern, K.T. Nguyen, Y. Hong, Biodegradable Nanoparticles Enhanced Adhesiveness of Mussel-Like Hydrogels at Tissue Interface, Adv. Healthc. Mater. 7 (2018) 1–9, doi:10.1002/adhm.201701069.
[30] B.T. Jung, M. Lim, K. Jung, M. Li, H. Dong, N. Dube, T. Xu, Designing sub-20 nm self-assembled nanocarriers for small molecule delivery: interplay among structural geometry, assembly energetics, and cargo release kinetics, J. Control. Release. 329 (2021) 538–551, doi:10.1016/j.jconrel.2020.09.037.
[31] V. Drebezghova, H. Gojzewski, A. Allal, M.A. Hempenius, C. Nardin, G.J. Vancso, Network Mesh Nanostructures in Cross-Linked Poly(Dimethylsiloxane) Visualized by AFM, Macromol. Chem. Phys. 221 (2020) 1–7, doi:10.1002/macp.202000170.
[32] D. Calvet, J.Y. Wong, S. Giasson, Rheological monitoring of polyacrylamide gelation: importance of cross-link density and temperature, Macromolecules 37 (2004) 7762–7771, doi:10.1021/ma049072r.
[33] A.A. Martí i Líndez, W. Reith, Arginine-dependent immune responses, Cell. Mol. Life Sci. 78 (2021) 5303–5324, doi:10.1007/s00018-021-03828-4.
[34] C. Wu, Y. Xue, P. Wang, L. Lin, Q. Liu, N. Li, J. Xu, X. Cao, IFN-γ primes macrophage activation by increasing phosphatase and tensin homolog via downregulation of miR-3473b, J. Immunol. 193 (2014) 3036–3044, doi:10.4049/jimmunol.1302379.
[35] T. Roszer, Understanding the Mysterious M2 Macrophage through Activation Markers and Effector Mechanisms, Mediators Inflamm (2015) 1–16, doi:10.32388/n35phw.
[36] R. Wakabayashi, H. Kono, S. Kozaka, Y. Tahara, N. Kamiya, M. Goto, Transcutaneous codelivery of tumor antigen and resiquimod in solid-in-oil nanodispersions promotes antitumor immunity, ACS Biomater. Sci. Eng. 5 (2019) 2297–2306, doi:10.1021/acsbiomaterials.9b00260.
[37] C.E. Brubaker, P.B. Messersmith, Enzymatically degradable mussel-inspired adhesive hydrogel, Biomacromolecules 12 (2011) 4326–4334, doi:10.1021/bm201261d.
[38] A.C. Gladman, Toxicodendron dermatitis: poison ivy, oak, and sumac, Wilderness Environ. Med. 17 (2006) 120–128, doi:10.1580/PR31-05.1.
[39] J. Guo, T. Suma, J.J. Richardson, H. Ejima, Modular Assembly of Biomaterials Using Polyphenols as Building Blocks, ACS Biomater. Sci. Eng. (2019), doi:10.1021/acsbiomaterials.8b01507.
[40] L. Han, X. Lu, K. Liu, K. Wang, L. Fang, L.-.T. Weng, H. Zhang, Y. Tang, F. Ren, C. Zhao, Mussel-inspired adhesive and tough hydrogel based on nanoclay confined dopamine polymerization, ACS Nano. 11 (2017) 2561–2574, doi:10.1021/acsnano.6b05318.
[41] D. Gan, T. Xu, W. Xing, X. Ge, L. Fang, K. Wang, F. Ren, X. Lu, Mussel-Inspired Contact-Active Antibacterial Hydrogel with High Cell Affinity, Toughness, and Recoverability, Adv. Funct. Mater. 29 (2019) 1–11, doi:10.1002/adfm.201805964.
[42] J. Shin, J.S. Lee, C. Lee, H. Park, K. Yang, Y. Jin, J.H. Ryu, K.S. Hong, S. Moon, H. Chung, Tissue adhesive catechol-modified hyaluronic acid hydrogel for effective, minimally invasive cell therapy, Adv. Funct. Mater. 25 (2015) 3814–3824, doi:10.1002/adfm.201500006.
[43] K. Chen, Q. Lin, L. Wang, Z. Zhuang, Y. Zhang, D. Huang, H. Wang, An All-in-One Tannic Acid-Containing Hydrogel Adhesive with High Toughness, Notch Insensitivity, Self-Healability, Tailorable Topography, and Strong, Instant, and On-Demand Underwater Adhesion, ACS Appl. Mater. Interfaces (2021), doi:10.1021/acsami.1c00637.
[44] A.N.F. Versypt, D.W. Pack, R.D. Braatz, Mathematical modeling of drug delivery from autocatalytically degradable PLGA microspheres—A review, J. Control. Release. 165 (2013) 29–37, doi:10.1016/j.jconrel.2012.10.015.
[45] G.A. Roth, V.C.T.M. Picece, B.S. Ou, W. Luo, B. Pulendran, E.A. Appel, Designing spatial and temporal control of vaccine responses, Nat. Rev. Mater. 7 (2022) 174–195, doi:10.1038/s41578-021-00372-2.
[46] H. Ejima, J.J. Richardson, F. Caruso, Metal-phenolic networks as a versatile platform to engineer nanomaterials and biointerfaces, Nano Today 12 (2017) 136–148, doi:10.1016/j.nantod.2016.12.012.
[47] M.R. Prausnitz, Microneedles for transdermal drug delivery, Adv. Drug Deliv. Rev. 56 (2004) 581–587, doi:10.1016/j.addr.2003.10.023.
[48] S.A. Machekposhti, M. Soltani, P. Najafizadeh, S.A. Ebrahimi, P. Chen, Biocompatible polymer microneedle for topical/dermal delivery of tranexamic acid, J. Control. Release. 261 (2017) 87–92, doi:10.1016/j.jconrel.2017.06.016.
[49] Q. Chen, C. Wang, X. Zhang, G. Chen, Q. Hu, H. Li, J. Wang, D. Wen, Y. Zhang, Y. Lu, G. Yang, C. Jiang, J. Wang, G. Dotti, Z. Gu, In situ sprayed bioresponsive immunotherapeutic gel for post-surgical cancer treatment, Nat. Nanotechnol. 14 (2019) 89–97, doi:10.1038/s41565-018-0319-4.
[50] J. Stahl, M. Wohlert, M. Kietzmann, Microneedle pretreatment enhances the percutaneous permeation of hydrophilic compounds with high melting points, BMC Pharmacol. Toxicol. 13 (2012) 5, doi:10.1186/2050-6511-13-5.
[51] M. Singh, A. Chakrapani, D. O'Hagan, Nanoparticles and microparticles as vaccine-delivery systems, Expert Rev. Vaccines. 6 (2007) 797–808, doi:10.1586/14760584.6.5.797.